Metal–Organic Frameworks

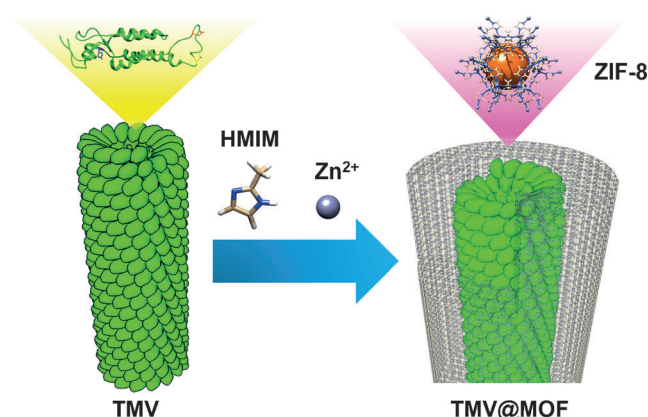# Template-Directed Synthesis of Porous and Protective Core–Shell Bionanoparticles

Shaobo Li, Madushani Dharmarwardana, Raymond P. Welch, Yixin Ren, Christina M. Thompson, Ronald A. Smaldone, and Jeremiah J. Gassensmith*

Abstract: Metal–organic frameworks (MOFs) are promising high surface area coordination polymers with tunable pore structures and functionality; however, a lack of good size and morphological control over the as-prepared MOFs has persisted as an issue in their application. Herein, we show how a robust protein template, tobacco mosaic virus (TMV), can be used to regulate the size and shape of as-fabricated MOF materials. We were able to obtain discrete rod-shaped TMV@MOF core–shell hybrids with good uniformity, and their diameters could be tuned by adjusting the synthetic conditions, which can also significantly impact the stability of the core–shell composite. More interestingly, the virus particle underneath the MOF shell can be chemically modified using a standard bioconjugation reaction, showing mass transportation within the MOF shell.

Metal–organic frameworks (MOFs) are a family of microporous crystalline materials with high specific surface areas and extended porosities, which have attained a level of preeminence because of their synthetic tunability. A MOF is constructed by coordinating rigid organic struts to a metal ion or cluster node to form a crystalline material with a defined pore structure, pore size, and chemical composition.[1] The seemingly infinite combination of metal nodes and organic struts has enabled highly tunable design strategies for specific needs,[2] such as gas storage,[3] sensing,[4] catalysis,[5] energy,[6] and in biomedical applications.[7] An issue arising in many of these applications, however, has been the difficulty in controlling the crystallite morphology, which typically yields bulk MOF powders with relatively large crystal size, random shape, and poor monodispersity. There is an articulated[8] interest in controlling the morphology of MOF crystallites because of the need for nanometer scale uniformity in biomedical and optoelectronics applications. The synthetic strategies so far employed to regulate the size and morphology of MOF crystals have generally involved the addition of metal-binding reagents such as ligands, surfactants, or polymers with chelating functional moieties.[9] Although these strategies afford regulation of size, the as-obtained MOF

particles are typically several hundred nanometers in size. More recently, MOF core–shell nanoparticles in the 100 nm range with good monodispersity have emerged,[10] though control over shape is not always high, resulting in irregular spheres or cubes.

Virus nanoparticles offer a level of control unavailable in synthetic systems as the surface chemistry can be altered by either chemical or genetic manipulation.[11] We selected the tobacco mosaic virus (TMV), a tubular viral particle that contains 2130 identical coat proteins self-assembled around a single strand of RNA. Because it is 300 nm long and only 18 nm wide, the anisotropy of the virus has made it an attractive target for applications in photonics,[12] light harvesting solar arrays,[13] and MRI contrast agents.[14] TMV is also attractive because it can be isolated in gram quantities from a kilogram of tobacco leaves. Each coat protein possesses solvent-accessible amino acid residues—tyrosine on the exterior and glutamates on the interior—and these anionic residues have been shown to be available for chemical conjugation.[15] Furthermore, the robustness of TMV has allowed it to play a versatile role as a bio-template for fabrication of organic or inorganic materials[16], and we reasoned that these qualities would make it useful in the production of core–shell bionanoparticle (CSBN) MOF frameworks with tightly regulated shell thickness, width, and length. To obtain aqueous-solution-stable CSBNs using MOFs, we turned to hydrolytically stable ZIF-8,[17] which is formed from the coordination of methyl imidazole ligands (HMIM) and Zn, and has recently been shown to nucleate and grow on enzymes—either naked[18] or polymer-coated[19]—in aqueous solution. Unlike enzymes, viruses are comparatively massive and are formed as highly symmetric

[*] S. Li, M. Dharmarwardana, R. P. Welch, Y. Ren, Dr. C. M. Thompson, Prof. R. A. Smaldone, Prof. J. J. Gassensmith
Department of Chemistry and Biochemistry
The University of Texas at Dallas
800 W Campbell Rd, Richardson, TX 75080 (USA)
E-mail: gassensmith@utdallas.edu
Homepage: http://gassensmithlab.com

Scheme 1. Synthesis and formation of TMV@ZIF-8 rod-shaped nanocomposites.

These are not the final page numbers!

quaternary structures; thus, we hypothesized they would give rise to regular nanoscopic shapes (Scheme 1).

Herein, we show that, using TMV as a template, the as-fabricated TMV@ZIF-8 retained the highly anisotropic rod shape of the parent virus. We were able to tune the thickness of the MOF shell by modifying the synthetic conditions. The as-obtained TMV@ZIF-8 composite demonstrates good stability in organic solvents and at high temperature. The surface-exposed tyrosine groups of the TMV remain reactive while inside the MOF shell and coupling reactions performed through the MOF do not undermine the integrity of the rod-shaped hybrids. Most strikingly, even after immersing the TMV@ZIF-8 in pure methanol overnight, we were able to remove the ZIF-8 shell and show that the virus itself could be reclaimed undamaged under these highly denaturing conditions.

For our initial experiments, a desalted virus solution was mixed with an aqueous solution of HMIM. Upon addition of an aliquot of $Zn(OAc)_2$ the reaction mixture immediately became turbid followed by flocculate formation. After 16 hours, the centrifuged solid was washed with ultrapure water twice to obtain an off-white suspension in water. We were initially pleased to find the anticipated rod structures by SEM but then frustrated to discover that the rods were very unstable; when removed from the mother liquor solution containing Zn and HMIM and placed in deionized (DI) water they collapsed into flaky cubes overnight (Supporting Information, Figure S1 b). From powder X-ray diffraction (PXRD) analysis of the as-synthesized rods, we observed that the shells contained the expected ZIF-8, but also reflections corresponding to a significant amount of crystalline $Zn(OAc)_2$ were observed (Supporting Information, Figure S2). This led us to conduct an investigation into the optimization of our synthetic conditions to reduce unwanted $Zn(OAc)_2$ growth and improve the stability of our rod composites. As a result of this investigation, we found that we could greatly affect not only the physical stability of the composites but also the shell thickness. A key observation was that when the HMIM:Zn molar ratio was low, the TMV@ZIF-8 core–shell composites had thinner shells and, conversely, at higher HMIM:Zn ratios, the shells thickened.

Two representative products of this investigation are presented in Figure 1, denoted as TZ-thin (micrographs shown in Figure 1a and b) and TZ-thick (Figure 1c and d). Synthetically, these two composites are differentiated by the HMIM:Zn molar ratio used in their preparation. Specifically, the TZ-thin composite was prepared from a 20:1 ratio and the thicker wall of TZ-thick was obtained when that ratio was increased to 40:1. SEM analysis shows that both composites form regular and homogenous rods with very tightly controlled thickness. TZ-thin, for instance, is 70 nm in diameter and TZ-thick is 100 nm. We could control the surface coating of the TMV@ZIF-8 as well by changing the concentration used in drop casting. The dense forests shown in the SEM images are a result of drop casting at high concentrations. Furthermore, we could isolate more discrete rods, even single rods, at lower concentrations (see the Supporting Information, Figure S3 and Figure 1 high magnification insets). TEM shows the viral interior, which arises from the low-contrast
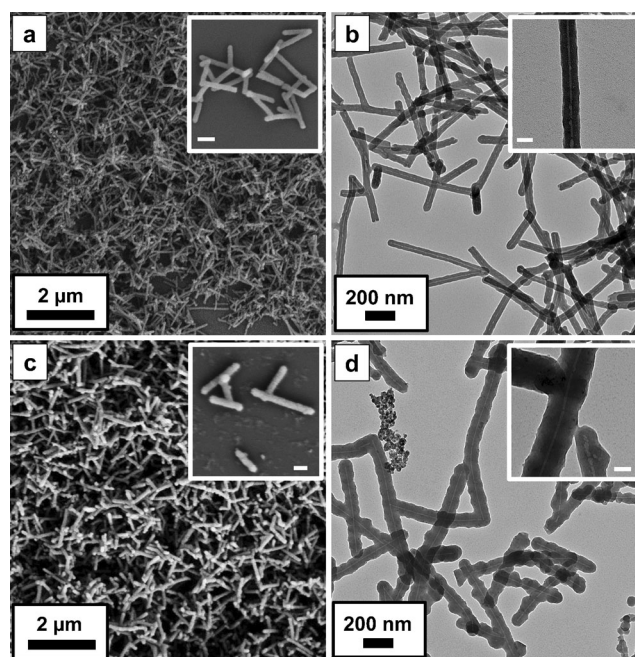
Figure 1. a) SEM and b) TEM of as-synthesized TZ-thin. c) SEM and d) TEM of as-synthesized TZ-thick. Inset scale bar: a), c) 200 nm; b), d) 50 nm.

TMV rod residing within the shell (Figure 1b and d). This provides direct evidence of successful ZIF-8 encapsulation of the tubular virus particle. We also observed rods much longer than 300 nm by SEM and TEM. This arises from TMV's propensity to align head-to-tail.[16a,d] This phenomenon is illustrated in the inset of Figure 1d, which shows one of these supramolecular junctions in which the virus particles line up in a head-to-tail fashion.

Crystallinity was confirmed by PXRD analysis showing reflections in excellent agreement with the simulated ZIF-8 pattern (Figure 2a). Thermogravimetric analysis (Figure 2b) under an air atmosphere shows a two-stage weight loss in both TZ-thin and TZ-thick, from 250 to 350 °C, which we attributed to the decomposition of the proteins, then a sharp decrease at 450 °C consistent with the decomposition of pure ZIF-8. The permanent porosity of the resulting shell was confirmed by nitrogen absorption analysis at 77 K (Figure 2c). The final BET surface-area values of the separate composites show an expected decrease in available surface area associated with the incorporation of the virus. The solution stability and synthetic yield were analyzed by functionalizing the inner channel of the TMV with a fluorescent FITC tag (fTMV, see the Supporting Information) and then growing the ZIF-8 shell around the resulting virus. After the growth and centrifugation of the composite, we found nearly undetectable levels of fluorescence remaining in the growth solution (Figure 2d, inset 1), indicating a nearly quantitative capture of fTMV. To determine if TMV could escape from the ZIF-8 and re-enter the solution, we monitored the fluorescence of a fTMV@ZIF-8 solution (Figure 2d, inset 2) over 24 h. As shown in Figure 2d the fluorescence did not increase until the shell was removed by
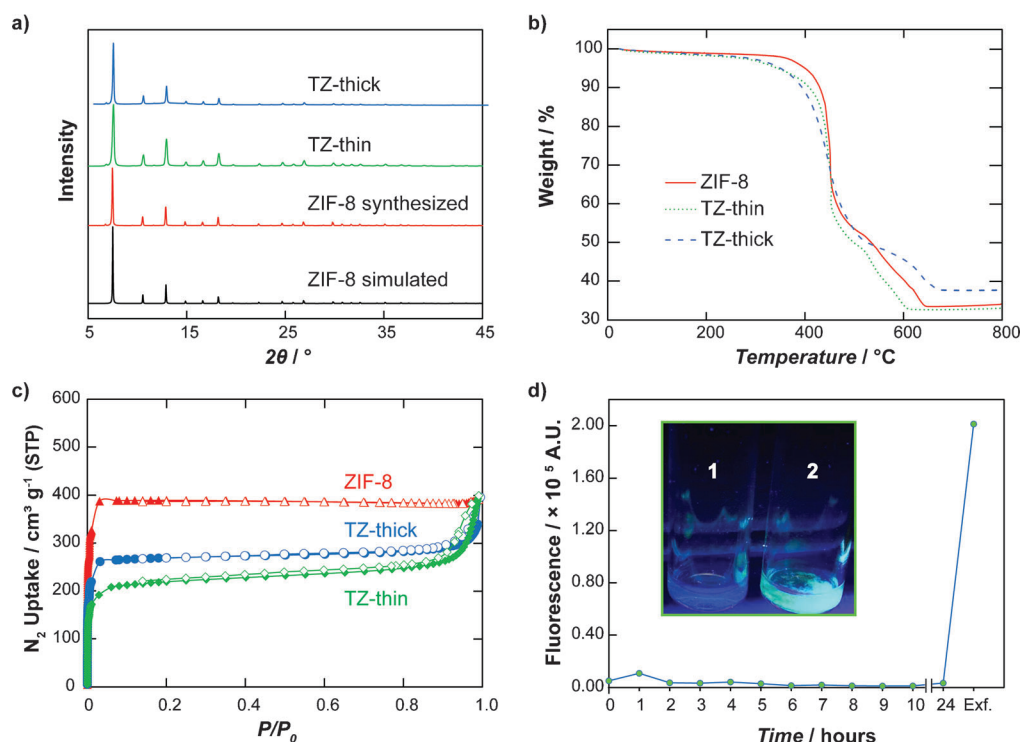
Figure 2. a) PXRD of simulated ZIF-8, synthesized ZIF-8, TZ-thin, and TZ-thick. b) TGA curves of ZIF-8, TZ-thin, and TZ-thick obtained in air atmosphere. c) N_2 sorption isotherm of ZIF-8, TZ-thin, and TZ-thick. The calculated BET surface area of ZIF-8, TZ-thick, and TZ-thin is 1537, 1053, and 847 $m^2 g^{-1}$, respectively. d) Fluorescence measurement of the solution after centrifugation at each time point and after exfoliation of ZIF-8 (Exf.); inset: 1) growth solution and 2) fTMV@ZIF-8 under UV light.

treatment with EDTA, indicating that the TMV was unable to leave the ZIF-8 shell and enter into the solution. These results clearly indicate that ZIF-8 shell growth is both high-yielding and robust.

An advantage of encapsulating biomaterials has been stability[18b] against environmental stressors such as organic solvents and high temperature, which would typically denature a protein. The stability of the resultant TZ-thin and TZ-thick composites were thus tested by immersing them in organic solvents of varying polarities. After a 16 h immersion, we looked at the resulting rods by SEM to confirm that the composites retained their distinctive morphology (Figure 3 and the Supporting Information, Figure S14). Both composites fared well in polar solvents (methanol and DMF) and, quite remarkably, TZ-thick endured immersion in DCM[20] without structural degradation, whereas TZ-thin recrystallized into cuboid particles of ZIF-8 (Figure 3c and g). We were able to further demonstrate the structural stability of TZ-thick by showing that the rod-shape of the composite was largely retained even after immersion in boiling water for 20 min (Figure 3h). Furthermore, we were able to recover the intact virus after immersing the composite in methanol for 16 h by exfoliating the MOF shell using an aqueous solution of EDTA. Without the ZIF-8 shell, methanol rapidly turns TMV into a slimy gel (Supporting Information, Figures S15 and S16). These results demonstrate that a thick MOF shell serves as a robust chainmail for the viral template against a denaturing solvent.[21]

A key advantage of MOFs is their permanent porosity, and the strategies hitherto used to create biomimetically mineralized shells on TMV essentially use the protein core as a sacrificial template. This means that the functional-group-rich surface under the shell is no longer accessible. Since ZIF-8 contains pores that allow for the diffusion of small molecules,[22] we wondered whether we could still perform bioconjugation reactions on the TMV surface in TMV@ZIF-8. We attempted a classic diazonium coupling reaction[23] to ascertain if the viral core is capable of post-functionalization after formation of the crystalline MOF shell. The reaction procedure is illustrated in Figure 4a. A solution of *p*-nitrobenzene diazonium salt was mixed with TZ-thin solution at 0°C. The whitish starting material quickly turned orange, indicating the formation of a nitrobenzyl diazo dye on the surface of the virus. After 30 min, the reaction mixture was centrifuged and the mother liquor was decanted. The solid was thoroughly washed with DI water and then suspended in glacial acetic acid to dissolve ZIF-8 and precipitate the RNA for analysis by ESI-MS. The deconvoluted mass spectrum, shown in Figure 4c, shows two intense peaks at 17 533 Da and 17 682 Da corresponding to unfunctionalized native coat protein and coat protein functionalized with the diazo dye, respectively. Curiously, when the reaction was repeated on TZ-thick,[24] the yield increased (Figure 4d). This was a slightly surprising result considering that the shell is thicker. Following removal of the ZIF-8 shell with EDTA, we confirmed by TEM that TZ-thick retained its quaternary structure after the bioconjugation reaction. As shown in the
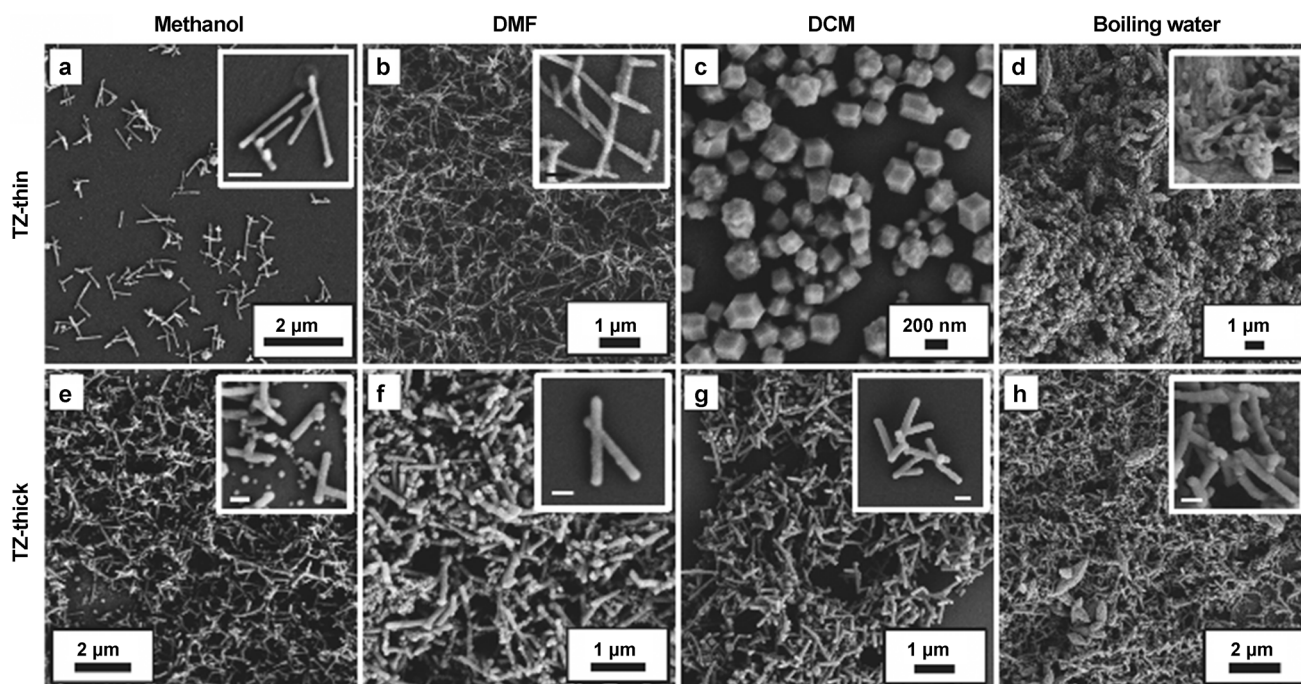
Figure 3. SEM of TZ-thin after immersion in a) methanol, b) DMF, c) DCM for 16 h, and in d) boiling water for 20 min. TZ-thick after immersion in e) methanol, f) DMF, g) DCM for 16 h, and in h) boiling water for 20 min. Inset scale bar: a) 300 nm; b, d, e, f, g, and h) 200 nm.
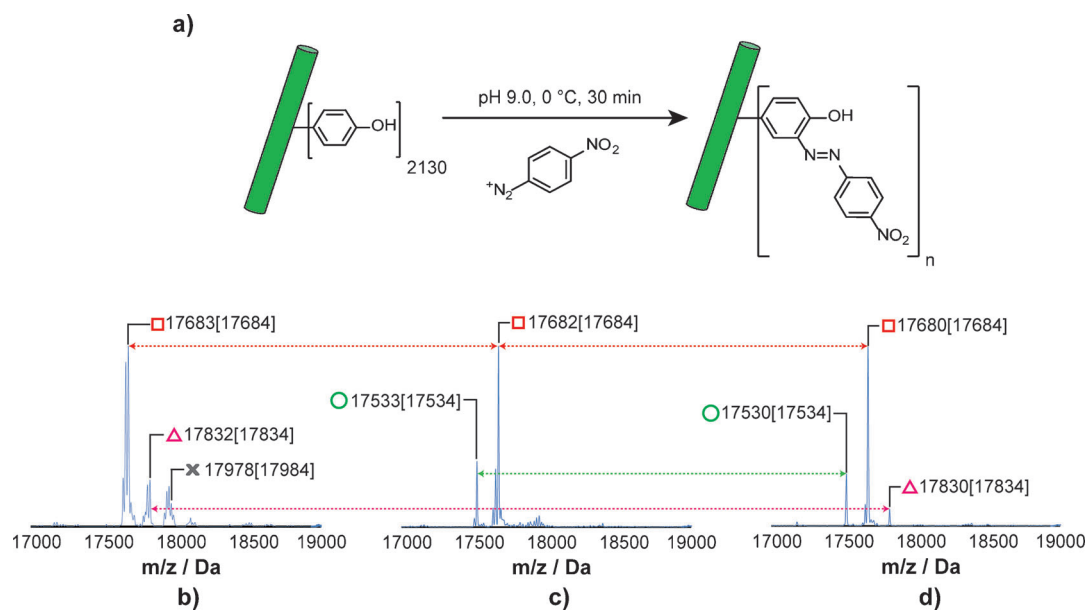
Figure 4. a) Diazonium coupling reaction on a tyrosine group on TMV. ESI-MS spectrum of TMV coat protein obtained from b) native TMV, c) TZ-thin, and d) TZ-thick after diazonium coupling reaction; theoretical mass is quoted for unmodified coat protein (○), coat protein with one (□), two (△), and three (**X**) functionalized residues.

Supporting Information, Figure S12c–f, viral particles stay intact after reaction and exfoliation with EDTA.

In conclusion, we have successfully prepared TMV@ZIF-8 rod-shaped CSBNs with tunable shell thickness. Morphological (shell thickness) control is possible by tuning the ligand:metal ratio during the shell-growth phase. The rod-like core–shell composites are stable in polar organic solvents for 16 h. The core–shell particles with thicker shells show extended stability in low polarity organic solvents and at higher temperature. Post-functionalization on the viral exterior using a diazonium coupling reaction is possible, demonstrating that these materials will likely have value to a broad audience. Our synthetic strategy not only provides a novel method for size and morphological control of MOF core–shell systems but also improves the stability of TMV without losing functionalizability of the surface-exposed tyrosine residues.

We envision that this synthetic strategy will allow the design and fabrication of one-dimensional high aspect ratio nanoparticles with more sophisticated functionalities accompanied with mass storage or transfer. This novel prototype may benefit applications such as drug delivery, imaging, sensing, and catalysis.

[1] a) O. M. Yaghi, M. O'Keeffe, N. W. Ockwig, H. K. Chae, M. Eddaoudi, J. Kim, *Nature* **2003**, *423*, 705–714; b) H. Furukawa, K. E. Cordova, M. O'Keeffe, O. M. Yaghi, *Science* **2013**, *341*, 1230444.

[2] a) O. K. Farha, C. E. Wilmer, I. Eryazici, B. G. Hauser, P. A. Parilla, K. O'Neill, A. A. Sarjeant, S. T. Nguyen, R. Q. Snurr, J. T. Hupp, *J. Am. Chem. Soc.* **2012**, *134*, 9860–9863; b) R. J. Marshall, S. L. Griffin, C. Wilson, R. S. Forgan, *J. Am. Chem. Soc.* **2015**, *137*, 9527–9530.

[3] a) Y. Peng, V. Krungleviciute, I. Eryazici, J. T. Hupp, O. K. Farha, T. Yildirim, *J. Am. Chem. Soc.* **2013**, *135*, 11887–11894; b) F. Gándara, H. Furukawa, S. Lee, O. M. Yaghi, *J. Am. Chem. Soc.* **2014**, *136*, 5271–5274.

[4] a) G. Lu, O. K. Farha, W. Zhang, F. Huo, J. T. Hupp, *Adv. Mater.* **2012**, *24*, 3970–3974; b) C. He, K. Lu, W. Lin, *J. Am. Chem. Soc.* **2014**, *136*, 12253–12256.

[5] a) O. Karagiaridi, M. B. Lalonde, W. Bury, A. A. Sarjeant, O. K. Farha, J. T. Hupp, *J. Am. Chem. Soc.* **2012**, *134*, 18790–18796; b) J. M. Falkowski, T. Sawano, T. Zhang, G. Tsun, Y. Chen, J. V. Lockard, W. Lin, *J. Am. Chem. Soc.* **2014**, *136*, 5213–5216; c) J. E. Mondloch, M. J. Katz, W. C. Isley III, P. Ghosh, P. Liao, W. Bury, G. W. Wagner, M. G. Hall, J. B. DeCoste, G. W. Peterson, R. Q. Snurr, C. J. Cramer, J. T. Hupp, O. K. Farha, *Nat. Mater.* **2015**, *14*, 512–516.

[6] a) H.-J. Son, S. Jin, S. Patwardhan, S. J. Wezenberg, N. C. Jeong, M. So, C. E. Wilmer, A. A. Sarjeant, G. C. Schatz, R. Q. Snurr, O. K. Farha, G. P. Wiederrecht, J. T. Hupp, *J. Am. Chem. Soc.* **2013**, *135*, 862–869; b) K. M. Choi, H. M. Jeong, J. H. Park, Y.-B. Zhang, J. K. Kang, O. M. Yaghi, *ACS Nano* **2014**, *8*, 7451–7457.

[7] a) C. He, K. Lu, D. Liu, W. Lin, *J. Am. Chem. Soc.* **2014**, *136*, 5181–5184; b) D. Liu, C. Poon, K. Lu, C. He, W. Lin, *Nat. Commun.* **2014**, *5*, 4182; c) K. Lu, C. He, W. Lin, *J. Am. Chem. Soc.* **2014**, *136*, 16712–16715.

[8] M. Sindoro, N. Yanai, A.-Y. Jee, S. Granick, *Acc. Chem. Res.* **2014**, *47*, 459–469.

[9] a) W. Cho, H. J. Lee, M. Oh, *J. Am. Chem. Soc.* **2008**, *130*, 16943–16946; b) T. Tsuruoka, S. Furukawa, Y. Takashima, K. Yoshida, S. Isoda, S. Kitagawa, *Angew. Chem. Int. Ed.* **2009**, *48*, 4739–4743; *Angew. Chem.* **2009**, *121*, 4833–4837; c) J. Cravillon, R. Nayuk, S. Springer, A. Feldhoff, K. Huber, M. Wiebcke, *Chem. Mater.* **2011**, *23*, 2130–2141; d) A. Umemura, S. Diring, S. Furukawa, H. Uehara, T. Tsuruoka, S. Kitagawa, *J. Am. Chem. Soc.* **2011**, *133*, 15506–15513.

[10] a) L. He, Y. Liu, J. Liu, Y. Xiong, J. Zheng, Y. Liu, Z. Tang, *Angew. Chem. Int. Ed.* **2013**, *52*, 3741–3745; *Angew. Chem.* **2013**, *125*, 3829–3833; b) P. Hu, J. Zhuang, L.-Y. Chou, H. K. Lee, X. Y. Ling, Y.-C. Chuang, C.-K. Tsung, *J. Am. Chem. Soc.* **2014**, *136*, 10561–10564; c) K. Na, K. M. Choi, O. M. Yaghi, G. A. Somorjai, *Nano Lett.* **2014**, *14*, 5979–5983; d) W. Zhang, Z.-Y. Wu, H.-L. Jiang, S.-H. Yu, *J. Am. Chem. Soc.* **2014**, *136*, 14385–14388; e) Z. Zhang, Y. Chen, X. Xu, J. Zhang, G. Xiang, W. He, X. Wang, *Angew. Chem. Int. Ed.* **2014**, *53*, 429–433; *Angew. Chem.* **2014**, *126*, 439–443; f) M. Zhao, K. Deng, L. He,

Y. Liu, G. Li, H. Zhao, Z. Tang, *J. Am. Chem. Soc.* **2014**, *136*, 1738–1741; g) J. Zhou, P. Wang, C. Wang, Y. T. Goh, Z. Fang, P. B. Messersmith, H. Duan, *ACS Nano* **2015**, *9*, 6951–6960.

[11] a) E. Strable, D. E. Prasuhn, A. K. Udit, S. Brown, A. J. Link, J. T. Ngo, G. Lander, J. Quispe, C. S. Potter, B. Carragher, D. A. Tirrell, M. G. Finn, *Bioconjugate Chem.* **2008**, *19*, 866–875; b) B. Schwarz, T. Douglas, *Wiley Interdiscip. Rev. Nanomed. Nanobiotechnol.* **2015**, *7*, 722–735; c) X. Zhao, Y. Lin, Q. Wang, *Wiley Interdiscip. Rev. Nanomed. Nanobiotechnol.* **2015**, *7*, 534–547; d) Z. Chen, N. Li, L. Chen, J. Lee, J. J. Gassensmith, *Small*, DOI:10.1002/smll.201601053; e) Z. Chen, N. Li, S. Li, M. Dharmarwardana, A. Schlimme, J. J. Gassensmith, *Wiley Interdiscip. Rev. Nanomed. Nanobiotechnol.* **2016**, *8*, 512–534.

[12] A. M. Wen, M. Infusino, A. De Luca, D. L. Kernan, A. E. Czapar, G. Strangi, N. F. Steinmetz, *Bioconjugate Chem.* **2015**, *26*, 51–62.

[13] R. A. Miller, N. Stephanopoulos, J. M. McFarland, A. S. Rosko, P. L. Geissler, M. B. Francis, *J. Am. Chem. Soc.* **2010**, *132*, 6068–6074.

[14] a) M. A. Bruckman, S. Hern, K. Jiang, C. A. Flask, X. Yu, N. F. Steinmetz, *J. Mater. Chem. B* **2013**, *1*, 1482–1490; b) M. A. Bruckman, L. N. Randolph, N. M. Gulati, P. L. Stewart, N. F. Steinmetz, *J. Mater. Chem. B* **2015**, *3*, 7503–7510.

[15] T. L. Schlick, Z. Ding, E. W. Kovacs, M. B. Francis, *J. Am. Chem. Soc.* **2005**, *127*, 3718–3723.

[16] a) W. Shenton, T. Douglas, M. Young, G. Stubbs, S. Mann, *Adv. Mater.* **1999**, *11*, 253–256; b) E. Dujardin, C. Peet, G. Stubbs, J. N. Culver, S. Mann, *Nano Lett.* **2003**, *3*, 413–417; c) M. Knez, M. Sumser, A. M. Bittner, C. Wege, H. Jeske, T. P. Martin, K. Kern, *Adv. Funct. Mater.* **2004**, *14*, 116–124; d) Z. Niu, J. Liu, L. A. Lee, M. A. Bruckman, D. Zhao, G. Koley, Q. Wang, *Nano Lett.* **2007**, *7*, 3729–3733; e) E. Royston, A. Ghosh, P. Kofinas, M. T. Harris, J. N. Culver, *Langmuir* **2008**, *24*, 906–912; f) E. Pomerantseva, K. Gerasopoulos, X. Chen, G. Rubloff, R. Ghodssi, *J. Power Sources* **2012**, *206*, 282–287.

[17] K. S. Park, Z. Ni, A. P. Côté, J. Y. Choi, R. Huang, F. J. Uribe-Romo, H. K. Chae, M. O'Keeffe, O. M. Yaghi, *Proc. Natl. Acad. Sci. USA* **2006**, *103*, 10186–10191.

[18] a) P. Chulkaivalsucharit, X. Wu, J. Ge, *RSC Adv.* **2015**, *5*, 101293–101296; b) K. Liang, R. Ricco, C. M. Doherty, M. J. Styles, S. Bell, N. Kirby, S. Mudie, D. Haylock, A. J. Hill, C. J. Doonan, P. Falcaro, *Nat. Commun.* **2015**, *6*, 7240; c) X. Wu, J. Ge, C. Yang, M. Hou, Z. Liu, *Chem. Commun.* **2015**, *51*, 13408–13411; d) X. Wu, C. Yang, J. Ge, Z. Liu, *Nanoscale* **2015**, *7*, 18883–18886; e) K. Liang, C. J. Coghlan, S. G. Bell, C. Doonan, P. Falcaro, *Chem. Commun.* **2016**, *52*, 473–476.

[19] a) F. Lyu, Y. Zhang, R. N. Zare, J. Ge, Z. Liu, *Nano Lett.* **2014**, *14*, 5761–5765; b) F.-K. Shieh, S.-C. Wang, C.-I. Yen, C.-C. Wu, S. Dutta, L.-Y. Chou, J. V. Morabito, P. Hu, M.-H. Hsu, K. C.-W. Wu, C.-K. Tsung, *J. Am. Chem. Soc.* **2015**, *137*, 4276–4279.

[20] The data show that these recrystallized particles are 200 to 300 nm in diameter, which is slightly shorter than the TMV@MOF rods that are mostly observed to be longer than 300 nm, indicating that the virus particles are likely not encapsulated in the crystals. Further studies are underway to determine whether protein is incarcerated inside. We observed the morphological change of TZ-thin in DCM using SEM. The micrographs indicate that within the first 40 min the rod-shape is retained; however, only polyhedral microcrystals are present after 3 h.

[21] S.-Y. Lee, J. S. Lim, J. N. Culver, M. T. Harris, *J. Colloid Interface Sci.* **2008**, *324*, 92–98.

[22] a) D. I. Kolokolov, L. Diestel, J. Caro, D. Freude, A. G. Stepanov, *J. Phys. Chem. C* **2014**, *118*, 12873–12879; b) H. Tanaka, S. Ohsaki, S. Hiraide, D. Yamamoto, S. Watanabe, M. T. Miyahara, *J. Phys. Chem. C* **2014**, *118*, 8445–8454; c) L. Zhang, G. Wu, J. Jiang, *J. Phys. Chem. C* **2014**, *118*, 8788–8794; d) D. I.

Kolokolov, A. G. Stepanov, H. Jobic, *J. Phys. Chem. C* **2015**, *119*, 27512–27520.

[23] M. A. Bruckman, N. F. Steinmetz in *Virus Hybrids as Nano-materials: Methods and Protocols* (Eds.: B. Lin, B. Ratna), Humana Press, Totowa, NJ, **2014**, pp. 173–185.

[24] Our current hypothesis on this difference in yield is that the thick MOF shell contains better crystallinity compared to the thin shell; thus, the thick ZIF shell possesses a higher order periodicity of the pore structure, which could facilitate the transport of small molecules.

6 www.angewandte.org

© 2016 Wiley-VCH Verlag GmbH & Co. KGaA, Weinheim

Angew. Chem. Int. Ed. **2016**, *55*, 1–7

↖↖ These are not the final page numbers!

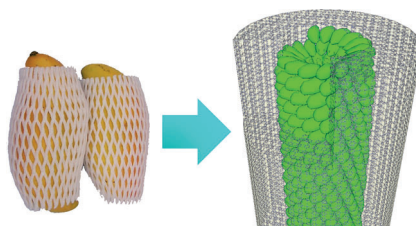## *Communications*

S. Li, M. Dharmarwardana, R. P. Welch,
Y. Ren, C. M. Thompson, R. A. Smaldone,
J. J. Gassensmith* —————— ▮▮▮–▮▮▮

Template-Directed Synthesis of Porous
and Protective Core–Shell
Bionanoparticles

It's a wrap: Sleeve netting provides a cost-effective solution to keep fresh fruits safe and sound. A metal–organic framework (MOF) is used to construct a molecular protective netting on the surface of the rod-like tobacco mosaic virus. The shell thickness was discovered to play a crucial role in the stability of the core–shell composite. More interestingly, the embedded virus particle can be chemically modified using a standard bioconjugation reaction, showing mass transportation within the MOF shell.

These are not the final page numbers! ↗↗